Composite Structures 94 (2011) 68–74

Contents lists available at SciVerse ScienceDirect

Composite Structures

journal homepage: www.elsevier.com/locate/compstruct

Hierarchical theories for the free vibration analysis of functionally graded beams

G. Giunta [a], D. Crisafulli [a,b,*], S. Belouettar [a], E. Carrera [b]

[a] Centre de Recherche Public Henri Tudor, 29, av. John F. Kennedy, L-1855, Luxembourg-Kirchberg, Luxembourg
[b] Politecnico di Torino, 24, c.so Duca degli Abruzzi, 10129, Turin, Italy

ARTICLE INFO

Article history:
Available online 11 August 2011

Keywords:
Beam structure
Hierarchical modelling
Closed form solution
Free vibration
Functionally graded material

ABSTRACT

This work addresses a free vibration analysis of functionally graded beams via several axiomatic refined theories. The material properties of the beam are assumed to vary continuously on the cross-section according to a power law distribution in terms of the volume fraction of the material constituents. Young's modulus, Poisson's ratio and density can vary along one or two dimensions all together or independently. The three-dimensional kinematic field is derived in a compact form as a generic *N*-order polynomial approximation. The governing differential equations and the boundary conditions are derived by variationally imposing the equilibrium via the Principle of Virtual Displacements. They are written in terms of a fundamental nucleo that does not depend upon the approximation order. A Navier-type, closed form solution is adopted. Higher-order displacements-based theories that account for non-classical effects are formulated. Classical beam models, such as Euler–Bernoulli's and Timoshenko's, are obtained as particular cases. Bending, torsion and axial modes are investigated. Slender as well as short beams are considered. Numerical results highlight the effect of different material distributions on natural frequencies and mode shapes and the accuracy of the proposed models.

1. Introduction

Many primary and secondary structural elements, such as helicopter rotor blades, robot arms and space erectable booms, can be idealised as beams. These structures play an important role in engineering fields (such as aeronautics and space) in which an effective and safe design is mandatory. The free vibration analysis of beams represents, therefore, an interesting and important research topic. The use of structures made from functionally graded materials (FGM) is increasing since a smooth variation of material properties along some preferred directions can improve the structural performance and solve some issues presented by composite materials. A continuous material properties variation, for instance, yields a continuous stress distribution within FGM structures. A brief overview of recent works about the free vibration of functionally graded beams is reported below. A fundamental frequency analysis of functionally graded (FG) beams with several boundary conditions has been carried out by Şimşek [1] using classical, first- and various higher-order shear deformation beam theories. Kapuria et al. [2] validated through experiments the static and free vibration response of layered FG beams. A third-order zig-zag theory in conjunction with the modified rule of mixtures for the effective modulus of elasticity was considered. Timoshenko's beam theory was adopted by Xiang and Yang [3] for the study of free and forced vibration of laminated FG beam of variable thickness under thermally induced initial stresses. Aydogdu and Taskin [4] investigated the free vibration of simply supported FG beam by different higher-order shear deformation and classical beam theories. Young's modulus varies in the thickness direction according to power and exponential laws. The static and dynamic behaviour of functionally graded beams was investigated by Li [5] adopting a unified approach for classical Euler–Bernoulli and Timoshenko beam theories. A first-order shear deformation beam theory was used by Sina et al. [6] to analyse the free vibration of functionally graded beams. The equations of motion were derived using Hamilton's principle. Different boundary conditions were considered. FG beam properties were assumed to be distributed according to a power law function of the volume fractions of the beam material constituents. The free vibration analysis of FG beams is investigated via the finite element method by Alshorbagy et al. [7]. Both axial and transverse material graduations based on a power law are considered. The system of equations of motion is derived by using the principle of virtual work under the assumptions of the Euler–Bernoulli beam theory. Murín et al. [8] considered a linear beam theory to establishing the equilibrium and kinematic equations of multi-layered FGM sandwich beams. The shear deformation and the effect of consistent mass distribution and mass inertia moment were accounted for. Results were compared with

* Corresponding author at: Department of Advanced Materials and Structures, Centre de Recherche Public Henri Tudor, 29, av. John F. Kennedy, L-1855, Luxembourg-Kirchberg, Luxembourg. Tel.: +352 54 55 80 479; fax: +352 42 59 91 555.
E-mail address: daniela.crisafulli@tudor.lu (D. Crisafulli).

0263-8223/$ - see front matter © 2011 Elsevier Ltd. All rights reserved.
doi:10.1016/j.compstruct.2011.07.016

those obtained using a commercial finite element model (FEM) code. A free vibration analysis of FGM beams via hierarchical models is addressed in this paper. These models are derived via a Unified Formulation (UF) that has been previously derived for plates and shells (see Carrera [9] and Carrera and Giunta [10,11]) and extended to beams with solid (see Giunta et al. [12], Carrera and Giunta [13] and Carrera et al. [14]) and thin-walled (see Giunta et al. [15]) cross-sections. Through a concise notation for the displacement field, the governing differential equations and the corresponding boundary conditions are reduced to a 'fundamental nucleo' that does not depend upon the approximation order. This latter can be assumed as a formulation free parameter. Displacement-based theories that account for non-classical effects, such as transverse shear and cross-section in- and out-of-plane warping, can be formulated. Flexural, torsional and axial natural frequencies are considered. Governing differential equations are solved via a Navier's, closed form solution. Slender and deep beams are investigated. Material gradation is considered through a power law function of either one or two cross-section coordinates. The proposed models are validated through comparison with three-dimensional FEM solutions. Numerical results show that very accurate results can be obtained with small computational costs.

2. Preliminaries

A beam is a structure whose axial extension (l) is predominant if compared to any other dimension orthogonal to it. The cross-section (Ω) is identified by intersecting the beam with planes that are orthogonal to its axis. A Cartesian reference system is adopted: y- and z-axis are two orthogonal directions laying on Ω. The x coordinate is coincident to the axis of the beam. It is bounded such that $0 \leqslant x \leqslant l$. Cross-section geometry and reference system are reported in Fig. 1. The cross-section is considered to be constant along x. The displacement field is:

$$\mathbf{u}^T(x,y,z) = \{\, u_x(x,y,z) \quad u_y(x,y,z) \quad u_z(x,y,z) \,\} \tag{1}$$

in which u_x, u_y and u_z are the displacement components along x-, y- and z-axes. Superscript 'T' represents the transposition operator. Stress, $\boldsymbol{\sigma}$, and strain, $\boldsymbol{\varepsilon}$, vectors are grouped into vectors $\boldsymbol{\sigma}_n$, $\boldsymbol{\varepsilon}_n$ that lay on the cross-section:

$$\boldsymbol{\sigma}_n^T = \{\, \sigma_{xx} \quad \sigma_{xy} \quad \sigma_{xz} \,\} \quad \boldsymbol{\varepsilon}_n^T = \{\, \varepsilon_{xx} \quad \varepsilon_{xy} \quad \varepsilon_{xz} \,\} \tag{2}$$

and $\boldsymbol{\sigma}_p$, $\boldsymbol{\varepsilon}_p$ laying on planes orthogonal to Ω:

$$\boldsymbol{\sigma}_p^T = \{\, \sigma_{yy} \quad \sigma_{zz} \quad \sigma_{yz} \,\} \quad \boldsymbol{\varepsilon}_p^T = \{\, \varepsilon_{yy} \quad \varepsilon_{zz} \quad \varepsilon_{yz} \,\} \tag{3}$$

Under the hypothesis of linear analysis, the following strain–displacement geometrical relations hold:

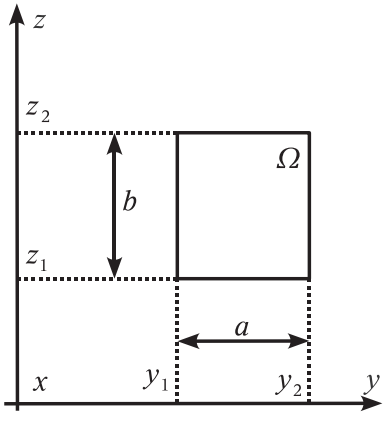

Fig. 1. Beam cross-section geometry and reference system.

$$\begin{aligned} \boldsymbol{\varepsilon}_n^T &= \{\, u_{x,x} \quad u_{x,y} + u_{y,x} \quad u_{x,z} + u_{z,x} \,\} \\ \boldsymbol{\varepsilon}_p^T &= \{\, u_{y,y} \quad u_{z,z} \quad u_{y,z} + u_{z,y} \,\} \end{aligned} \tag{4}$$

Subscripts 'x', 'y' and 'z', when preceded by comma, represent derivation versus the corresponding spatial coordinate. A compact vectorial notation can be adopted for Eq. (4):

$$\begin{aligned} \boldsymbol{\varepsilon}_n &= \mathbf{D}_{np}\mathbf{u} + \mathbf{D}_{nx}\mathbf{u} \\ \boldsymbol{\varepsilon}_p &= \mathbf{D}_p\mathbf{u} \end{aligned} \tag{5}$$

where $\mathbf{D}_{np}$, $\mathbf{D}_{nx}$, and $\mathbf{D}_p$ are the following differential matrix operators:

$$\mathbf{D}_{np} = \begin{bmatrix} 0 & 0 & 0 \\ \frac{\partial}{\partial y} & 0 & 0 \\ \frac{\partial}{\partial z} & 0 & 0 \end{bmatrix} \quad \mathbf{D}_{nx} = \mathbf{I}\frac{\partial}{\partial x} \quad \mathbf{D}_p = \begin{bmatrix} 0 & \frac{\partial}{\partial y} & 0 \\ 0 & 0 & \frac{\partial}{\partial z} \\ 0 & \frac{\partial}{\partial z} & \frac{\partial}{\partial y} \end{bmatrix} \tag{6}$$

$\mathbf{I}$ is the unit matrix. Under the hypothesis of linear elastic materials, the generalised Hooke law holds. According to Eqs. (2) and (3), it reads:

$$\begin{aligned} \boldsymbol{\sigma}_p &= \mathbf{C}_{pp}\boldsymbol{\varepsilon}_p + \mathbf{C}_{pn}\boldsymbol{\varepsilon}_n \\ \boldsymbol{\sigma}_n &= \mathbf{C}_{np}\boldsymbol{\varepsilon}_p + \mathbf{C}_{nn}\boldsymbol{\varepsilon}_n \end{aligned} \tag{7}$$

Matrices $\mathbf{C}_{pp}$, $\mathbf{C}_{pn}$, $\mathbf{C}_{np}$ and $\mathbf{C}_{nn}$ in Eq. (7) are:

$$\mathbf{C}_{pp} = \begin{bmatrix} C_{22} & C_{23} & 0 \\ C_{23} & C_{33} & 0 \\ 0 & 0 & C_{44} \end{bmatrix} \quad \mathbf{C}_{pn} = \mathbf{C}_{np}^T = \begin{bmatrix} C_{12} & 0 & 0 \\ C_{13} & 0 & 0 \\ 0 & 0 & 0 \end{bmatrix}$$
$$\mathbf{C}_{nn} = \begin{bmatrix} C_{11} & 0 & 0 \\ 0 & C_{66} & 0 \\ 0 & 0 & C_{55} \end{bmatrix} \tag{8}$$

In the case of isotropic FGMs, coefficients C_{ij} are:

$$\begin{aligned} C_{11} = C_{22} = C_{33} &= \frac{1-\nu}{(1+\nu)(1-2\nu)}E \quad C_{12} = C_{13} = C_{23} \\ &= \frac{\nu}{(1+\nu)(1-2\nu)}E \quad C_{44} = C_{55} = C_{66} = \frac{1}{2(1+\nu)}E \end{aligned} \tag{9}$$

being Young's modulus (E) and Poisson's ratio (ν) function of the position above the cross-section. The generic material property f is assumed to vary versus y or/and z coordinate according to a power law distribution:

$$f = (f_1 - f_2)(\alpha_y y + \beta_y)^{n_y}(\alpha_z z + \beta_z)^{n_z} + f_2 \tag{10}$$

This gradation law is obtained through the assumption of a power gradation law of the volume fraction of two constituent materials and the rule of mixtures, see Reddy [16] and Chakraborty et al. [17].

3. Hierarchical beam theories

The variation of the displacement field over the cross-section can be postulated a priori. Several displacement-based theories can be formulated on the basis of the following generic kinematic field:

$$\mathbf{u}(x,y,z) = F_\tau(y,z)\mathbf{u}_\tau(x) \quad \text{with } \tau = 1,2,\ldots,N_u \tag{11}$$

N_u stands for the number of unknowns. It depends on the approximation order N that is a free parameter of the formulation. The compact expression is based on Einstein's notation: subscript τ indicates summation. Thanks to this notation, problem's governing differential equations and boundary conditions can be derived in terms of a single 'fundamental nucleo'. The complexity related to higher than classical approximation terms is tackled and the theoretical formulation is valid for the generic approximation order

and approximating functions $F_\tau(y,z)$. In this paper, the functions F_τ are assumed to be Mac Laurin's polynomials. This choice is inspired by the classical beam models. N_u and F_τ as functions of N can be obtained via Pascal's triangle as shown in Table 1. The actual governing differential equations and boundary conditions due to a fixed approximation order and polynomials type are obtained straightforwardly via summation of the nucleo corresponding to each term of the expansion. According to the previous choice of polynomial function, the generic, N-order displacement field is:

$$\begin{aligned} u_x &= u_{x1} + u_{x2}y + u_{x3}z + \cdots + u_{x_{\frac{(N^2+N+2)}{2}}}y^N + \cdots + u_{x_{\frac{(N+1)(N+2)}{2}}}z^N \\ u_y &= u_{y1} + u_{y2}y + u_{y3}z + \cdots + u_{y_{\frac{(N^2+N+2)}{2}}}y^N + \cdots + u_{y_{\frac{(N+1)(N+2)}{2}}}z^N \\ u_z &= u_{z1} + u_{z2}y + u_{z3}z + \cdots + u_{z_{\frac{(N^2+N+2)}{2}}}y^N + \cdots + u_{z_{\frac{(N+1)(N+2)}{2}}}z^N \end{aligned} \tag{12}$$

As far as the first-order approximation order is concerned, the kinematic field is:

$$\begin{aligned} u_x &= u_{x1} + u_{x2}y + u_{x3}z \\ u_y &= u_{y1} + u_{y2}y + u_{y3}z \\ u_z &= u_{z1} + u_{z2}y + u_{z3}z \end{aligned} \tag{13}$$

Classical models, such as Timoshenko beam theory (TB):

$$\begin{aligned} u_x &= u_{x1} + u_{x2}y + u_{x3}z \\ u_y &= u_{y1} \\ u_z &= u_{z1} \end{aligned} \tag{14}$$

and Euler–Bernoulli beam theory (EB):

$$\begin{aligned} u_x &= u_{x1} - u_{y1,x}y - u_{z1,x}z \\ u_y &= u_{y1} \\ u_z &= u_{z1} \end{aligned} \tag{15}$$

are straightforwardly derived from the first-order approximation model. In TB, no shear correction coefficient is considered, since it depends upon several parameters, such as the geometry of the cross-section (see, for instance, Cowper [18] and Murty [19]). Higher order models yield a more detailed description of the shear mechanics (no shear correction coefficient is required), of the in- and out-of-section deformations, of the coupling of the spatial directions due to Poisson's effect and of the torsional mechanics than classical models do. EB theory neglects them all, since it was formulated to describe the bending mechanics. TB model accounts for constant shear stress and strain components. In the case of classical models and first-order approximation, reduced material stiffness coefficients should be used due to Poisson's locking (see Carrera and Brischetto [20,21]).

4. Governing equations

The strong form of the governing differential equations and the boundary conditions are obtained via D'Alambert's Principle:

$$\delta L_i = \delta L_{in} \tag{16}$$

Table 1
Mac Laurin's polynomials terms via Pascal's triangle.

N	N_u	F_τ
0	1	$F_1 = 1$
1	3	$F_2 = y$ $F_3 = z$
2	6	$F_4 = y^2$ $F_5 = yz$ $F_6 = z^2$
3	10	$F_7 = y^3$ $F_8 = y^2z$ $F_9 = yz^2$ $F_{10} = z^3$
...	...	...
N	$\frac{(N+1)(N+2)}{2}$	$F_{\frac{(N^2+N+2)}{2}} = y^N$ $F_{\frac{(N^2+N+4)}{2}} = y^{N-1}z$ ... $F_{\frac{N(N+3)}{2}} = yz^{N-1}$ $F_{\frac{(N+1)(N+2)}{2}} = z^N$

δ stands for a virtual variation. L_i represents the strain energy. L_{in} stands for the inertial work.

4.1. Virtual variation of the strain energy

According to the grouping of the stress and strain components in Eqs. (2) and (3), the virtual variation of the strain energy is considered as sum of two contributes:

$$\delta L_i = \int_l \int_\Omega \left(\delta \boldsymbol{\epsilon}_n^T \boldsymbol{\sigma}_n + \delta \boldsymbol{\epsilon}_p^T \boldsymbol{\sigma}_p \right) d\Omega\, dx \tag{17}$$

By substitution of the geometrical relations, Eq. (5), the material constitutive equations, Eq. (7), and the unified hierarchical approximation of the displacements, Eq. (11), and after integration by parts, Eq. (17) reads:

$$\begin{aligned} \delta L_i = \int_l \delta \mathbf{u}_\tau^T \int_\Omega \Big[& -\mathbf{D}_{nx}^T \mathbf{C}_{np} F_\tau (\mathbf{D}_p F_s \mathbf{I}) - \mathbf{D}_{nx}^T \mathbf{C}_{nn} F_\tau (\mathbf{D}_{np} F_s \mathbf{I}) \\ & - \mathbf{D}_{nx}^T \mathbf{C}_{nn} F_\tau F_s \mathbf{D}_{nx} + (\mathbf{D}_{np} F_\tau \mathbf{I})^T \mathbf{C}_{np} (\mathbf{D}_p F_s \mathbf{I}) + (\mathbf{D}_{np} F_\tau \mathbf{I})^T \mathbf{C}_{nn} (\mathbf{D}_{np} F_s \mathbf{I}) \\ & + (\mathbf{D}_{np} F_\tau \mathbf{I})^T \mathbf{C}_{nn} F_s \mathbf{D}_{nx} + (\mathbf{D}_p F_\tau \mathbf{I})^T \mathbf{C}_{pp} (\mathbf{D}_p F_s \mathbf{I}) \\ & + (\mathbf{D}_p F_\tau \mathbf{I})^T \mathbf{C}_{pn} (\mathbf{D}_{np} F_s \mathbf{I}) + (\mathbf{D}_p F_\tau \mathbf{I})^T \mathbf{C}_{pn} F_s \mathbf{D}_{nx} \Big] d\Omega \mathbf{u}_s\, dx \\ & + \delta \mathbf{u}_\tau^T \int_\Omega F_\tau \left[\mathbf{C}_{np} (\mathbf{D}_p F_s \mathbf{I}) + \mathbf{C}_{nn} (\mathbf{D}_{np} F_s \mathbf{I}) + \mathbf{C}_{nn} F_s \mathbf{D}_{nx} \right] d\Omega \mathbf{u}_s \Big|_{x=0}^{x=l} \end{aligned} \tag{18}$$

In a compact vectorial form:

$$\delta L_i = \int_l \delta \mathbf{u}_\tau^T \overline{\mathbf{K}}^{\tau s}\, \mathbf{u_s}\, \mathbf{dx} + \left[\delta \mathbf{u}_\tau^T\, \overline{\mathbf{\Pi}}^{\tau s}\, \mathbf{u_s} \right]_{\mathbf{x=0}}^{\mathbf{x=l}} \tag{19}$$

The components of the differential linear stiffness matrix $\overline{\mathbf{K}}^{\tau s}$ are:

$$\begin{aligned} \overline{K}_{xx}^{\tau s} &= J_{\tau,y s,y}^{66} + J_{\tau,z s,z}^{55} - J_{\tau s}^{11} \frac{\partial^2}{\partial x^2} & \overline{K}_{xy}^{\tau s} &= \left(J_{\tau,y s}^{66} - J_{\tau s,y}^{12} \right) \frac{\partial}{\partial x} & \overline{K}_{xz}^{\tau s} &= \left(J_{\tau,z s}^{55} - J_{\tau s,z}^{13} \right) \frac{\partial}{\partial x} \\ \overline{K}_{yy}^{\tau s} &= J_{\tau,y s,y}^{22} + J_{\tau,z s,z}^{44} - J_{\tau s}^{66} \frac{\partial^2}{\partial x^2} & \overline{K}_{yx}^{\tau s} &= \left(J_{\tau,y s}^{12} - J_{\tau s,y}^{66} \right) \frac{\partial}{\partial x} & \overline{K}_{yz}^{\tau s} &= J_{\tau,y s,z}^{23} + J_{\tau,z s,y}^{44} \\ \overline{K}_{zz}^{\tau s} &= J_{\tau,y s,y}^{44} + J_{\tau,z s,z}^{33} - J_{\tau s}^{55} \frac{\partial^2}{\partial x^2} & \overline{K}_{zx}^{\tau s} &= \left(J_{\tau,z s}^{13} - J_{\tau s,z}^{55} \right) \frac{\partial}{\partial x} & \overline{K}_{zy}^{\tau s} &= J_{\tau,z s,y}^{23} + J_{\tau,y s,z}^{44} \end{aligned} \tag{20}$$

The generic term $J_{\tau_{(,\phi)} s_{(,\xi)}}^{gh}$ is a cross-section moment:

$$J_{\tau_{(,\phi)} s_{(,\xi)}}^{gh} = \int_\Omega C_{gh} F_{\tau_{(,\phi)}} F_{s_{(,\xi)}}\, d\Omega \tag{21}$$

and it is obtained via Gauss' integration. As far as the boundary conditions are concerned, the components of $\overline{\mathbf{\Pi}}^{\tau s}$ are:

$$\begin{aligned} \overline{\Pi}_{xx}^{\tau s} &= J_{\tau s}^{11} \frac{\partial}{\partial x} & \overline{\Pi}_{xy}^{\tau s} &= J_{\tau s,y}^{12} & \overline{\Pi}_{xz}^{\tau s} &= J_{\tau s,z}^{13} \\ \overline{\Pi}_{yy}^{\tau s} &= J_{\tau s}^{66} \frac{\partial}{\partial x} & \overline{\Pi}_{yx}^{\tau s} &= J_{\tau s,y}^{66} & \overline{\Pi}_{yz}^{\tau s} &= 0 \\ \overline{\Pi}_{zz}^{\tau s} &= J_{\tau s}^{55} \frac{\partial}{\partial x} & \overline{\Pi}_{zx}^{\tau s} &= J_{\tau s,z}^{55} & \overline{\Pi}_{zy}^{\tau s} &= 0 \end{aligned} \tag{22}$$

4.2. Virtual variation of the inertial work

The virtual variation of the inertial work is:

$$\delta L_{in} = \int_l \int_\Omega \rho \delta \mathbf{u} \ddot{\mathbf{u}}\, d\Omega\, dx \tag{23}$$

Double dots stand as second derivative versus time (t). Accounting for Eqs. (11), then (23) becomes:

$$\delta L_{in} = \int_l \delta \mathbf{u}_\tau^T \int_\Omega \rho F_\tau F_s d\Omega\, \ddot{\mathbf{u}}_s\, dx \tag{24}$$

and in a compact vectorial form:

$$\delta L_{in} = \int_l \delta \mathbf{u}_\tau^T \, \mathbf{M}^{\tau s} \ddot{\mathbf{u}}_s \, dx \tag{25}$$

The components of the inertial matrix $\mathbf{M}^{\tau s}$ are:

$$M_{ij}^{\tau s} = \delta_{ij} J_{\tau s}^{\rho} \quad \text{with } i,j = x,y,z \tag{26}$$

where δ_{ij} is Kronecker's delta and:

$$J_{\tau s}^{\rho} = \int_\Omega \rho F_\tau F_s \, d\Omega \tag{27}$$

4.3. Governing equations' fundamental nucleo

The explicit form of the fundamental nucleo of the governing equations is:

$$\begin{aligned}
\delta u_{x\tau} &: -J_{\tau s}^{11} u_{xs,xx} + \left(J_{\tau,zs,z}^{55} + J_{\tau,ys,y}^{66}\right) u_{xs} + \left(J_{\tau,ys}^{66} - J_{\tau s,y}^{12}\right) u_{ys,x} \\
&\quad + \left(J_{\tau,zs}^{55} - J_{\tau s,z}^{13}\right) u_{zs,x} = J_{\tau s}^{\rho} \ddot{u}_{xs} \\
\delta u_{y\tau} &: \left(J_{\tau,ys}^{12} - J_{\tau s,y}^{66}\right) u_{xs,x} - J_{\tau s}^{66} u_{ys,xx} + \left(J_{\tau,ys,y}^{22} + J_{\tau,zs,z}^{44}\right) u_{ys} \\
&\quad + \left(J_{\tau,ys,z}^{23} + J_{\tau,zs,y}^{44}\right) u_{zs} = J_{\tau s}^{\rho} \ddot{u}_{ys} \\
\delta u_{z\tau} &: \left(J_{\tau,zs}^{13} - J_{\tau s,z}^{55}\right) u_{xs,x} + \left(J_{\tau,zs,y}^{23} + J_{\tau,ys,z}^{44}\right) u_{ys} - J_{\tau s}^{55} u_{zs,xx} \\
&\quad + \left(J_{\tau,zs,z}^{33} + J_{\tau,ys,y}^{44}\right) u_{zs} = J_{\tau s}^{\rho} \ddot{u}_{zs}
\end{aligned} \tag{28}$$

The boundary conditions are:

$$\begin{aligned}
&\delta u_{x\tau} \left(J_{\tau s}^{11} u_{xs,x} + J_{\tau s,y}^{12} u_{ys} + J_{\tau s,z}^{13} u_{zs}\right)\Big|_{x=0}^{x=l} = 0 \\
&\delta u_{y\tau} \left(J_{\tau s,y}^{66} u_{xs} + J_{\tau s}^{66} u_{ys,x}\right)\Big|_{x=0}^{x=l} = 0 \\
&\delta u_{z\tau} \left(J_{\tau s,z}^{55} u_{xs} + J_{\tau s}^{55} u_{zs,x}\right)\Big|_{x=0}^{x=l} = 0
\end{aligned} \tag{29}$$

For a fixed approximation order, the nucleo has to be expanded versus the indexes τ and s in order to obtain the governing equations and the boundary conditions of the desired model.

5. Closed form analytical solution

The differential equations are solved via a Navier-type solution. Simply supported beams are, therefore, investigated. The following harmonic displacement field is adopted:

$$\begin{aligned}
u_x &= U_{x\tau} F_\tau(y,z) \cos(\alpha x) e^{i\omega t} \\
u_y &= U_{y\tau} F_\tau(y,z) \sin(\alpha x) e^{i\omega t} \\
u_z &= U_{z\tau} F_\tau(y,z) \sin(\alpha x) e^{i\omega t}
\end{aligned} \tag{30}$$

where α is:

$$\alpha = \frac{m\pi}{l} \tag{31}$$

$m \in \mathbb{N} \setminus 0$ represents the half-wave number along the beam axis and i is the imaginary unit. $\{U_{i\tau} : i = x,y,z\}$ are the maximal amplitudes of the displacement components. The displacement field in Eq. (30) satisfies the boundary conditions since:

$$\begin{aligned}
&u_{x,x}(0) = u_{x,x}(l) = 0 \\
&u_y(0) = u_y(l) = 0 \\
&u_z(0) = u_z(l) = 0
\end{aligned} \tag{32}$$

Upon substitution of Eq. (30) into Eq. (28), the fundamental nucleo of the algebraic eigensystem is obtained:

$$\delta \mathbf{U}_\tau : (\mathbf{K}^{\tau s} - \omega^2 \mathbf{M}^{\tau s}) \mathbf{U}_s = 0 \tag{33}$$

The components of the linear stiffness matrix ($\mathbf{K}^{\tau s}$) are:

$$\begin{aligned}
K_{xx}^{\tau s} &= \alpha^2 J_{\tau s}^{11} + J_{\tau,zs,z}^{55} + J_{\tau,ys,y}^{66} \quad K_{xy}^{\tau s} = \alpha\left(J_{\tau,ys}^{66} - J_{\tau s,y}^{12}\right) \quad K_{xz}^{\tau s} = \alpha\left(J_{\tau,zs}^{55} - J_{\tau s,z}^{13}\right) \\
K_{yy}^{\tau s} &= \alpha^2 J_{\tau s}^{66} + J_{\tau,ys,y}^{22} + J_{\tau,zs,z}^{44} \quad K_{yx}^{\tau s} = \alpha\left(J_{\tau,ys}^{66} - J_{\tau s,y}^{12}\right) \quad K_{yz}^{\tau s} = J_{\tau,ys,z}^{23} + J_{\tau,zs,y}^{44} \\
K_{zz}^{\tau s} &= \alpha^2 J_{\tau s}^{55} + J_{\tau,zs,z}^{33} + J_{\tau,ys,y}^{44} \quad K_{zx}^{\tau s} = \alpha\left(J_{\tau s,z}^{55} - J_{\tau,zs}^{13}\right) \quad K_{zy}^{\tau s} = J_{\tau,zs,y}^{23} + J_{\tau,ys,z}^{44}
\end{aligned} \tag{34}$$

For a fixed approximation order, the eigensystem has to be assembled according to the summation indexes τ and s.

6. Numerical results and discussion

FGMs beams made of alumina and steel are considered. The mechanical properties of alumina are: $E_1 = 3.9 \times 10^5$ MPa, $\nu_1 = 0.25$, $\rho_1 = 3.96 \times 10^3$ kg/m^3. In the case of steel, the following mechanical properties are used: $E_2 = 2.1 \times 10^5$ MPa, $\nu_2 = 0.31$, $\rho_2 = 7.80 \times 10^3$ kg/m^3. E, ν and ρ vary along either y-axis or both y and z directions according to the power gradation law. Unless differently stated, a linear variation is considered in Eq. (10). Square cross-sections are considered. The sides of the cross-section are $a = b = 0.1$ m. The length-to-side ratio l/a is equal 100, 10 and five. Slender and deep beams are, therefore, investigated. The half-wave number m in Eq. (31) is assumed equal to one. Flexural, torsional and axial free vibration modes are investigated. Natural frequencies are put into the following dimensionless form:

$$\overline{\omega} = 10^2 \ \omega \ a \sqrt{\frac{\rho_2}{E_2}} \tag{35}$$

As far as validation is concerned, results (in terms of both natural frequencies and modes) are compared with three-dimensional FEM solutions obtained via the commercial code ANSYS, see ANSYS theory manual [22], Madenci and Guven [23] and Barbero [24]. The three-dimensional quadratic element "Solid95" is used. Each element is considered as homogeneous by referring to the material properties at its centre point. The accuracy of the three-dimensional FEM solution depends upon both the FEM numerical approximation and the approximation of the gradation law. In order to study the convergence of the three-dimensional reference solution, for each case three different meshes are considered. Acronym FEM 3D^a stand for a three-dimensional FEM model with 40 elements along the axial direction and 30 elements along y and z directions. Coarser solutions FEM 3D^b ($30 \times 20 \times 20$ elements) and FEM 3D^c ($20 \times 10 \times 10$ elements) are also considered. Although the three-dimensional FEM solution and the analytical one are different in nature, some considerations about computational time and effort can be addressed. For the reference FEM simulations, the computational time is as high as about two hours (refined mesh) and as low as about a minute (coarsest mesh). In the case of the proposed analytical solutions, the computational time is less than a second regardless the considered approximation order.

6.1. Material gradation along a cross-section direction

In this first example, material properties are supposed to vary along the y-axis only. Tables 2–4 present the dimensionless natural frequencies for $l/a = 100$, 10 and five. Mode I and II are two flexural modes on planes xz and xy, respectively. Mode III is a torsional mode and Mode IV is an axial one. Refined and coarsest three-dimensional solutions differ by less than about 0.1%. Increasing the number of degrees of freedom, the frequencies decrease since a less stiff model is considered. Considering five significant digits, the considered natural frequencies converge for an expansion

Table 2
Dimensionless natural frequencies, $E = E(y)$, $\nu = \nu(y)$, $\rho = \rho(y)$, $l/a = 100$, $n_1 = 1$.

$\overline{\omega}$	Mode I[1] $\times 10^2$	Mode II[2] $\times 10^2$	Mode III[3] $\times 1$	Mode IV[4] $\times 1$
FEM 3D[a]	3.8627	3.9217	2.4860	4.3247
FEM 3D[b]	3.8635	3.9223	2.4860	4.3247
FEM 3D[c]	3.8665	3.9244	2.4858	4.3247
$N \geqslant 8$	3.8623	3.9214	2.4861	4.3247
$N = 6, 7$	3.8623	3.9214	2.4868	4.3247
$N = 5$	3.8623	3.9214	2.4876	4.3247
$N = 4$	3.8624	3.9214	2.4877	4.3247
$N = 3$	3.8624	3.9214	2.7011	4.3247
$N = 2$	3.8639	3.9235	2.7080	4.3247
TB	3.8622	3.9215	–	4.3239
EB	3.8626	3.9219	–	4.3248

[1] Flexural mode on plane *xz*.
[2] Flexural mode on plane *xy*.
[3] Torsional mode.
[4] Axial mode.

Table 3
Dimensionless natural frequencies, $E = E(y)$, $\nu = \nu(y)$, $\rho = \rho(y)$, $l/a = 10$, $n_1 = 1$.

$\overline{\omega}$	Mode I[1] $\times 1$	Mode II[2] $\times 1$	Mode III[3] $\times 10^{-1}$	Mode IV[4] $\times 10^{-1}$
FEM 3D[a]	3.8027	3.8568	2.4872	4.3163
FEM 3D[b]	3.8029	3.8568	2.4872	4.3163
FEM 3D[c]	3.8038	3.8569	2.4870	4.3163
$N \geqslant 10$	3.8026	3.8568	2.4873	4.3163
$N = 8, 9$	3.8026	3.8568	2.4874	4.3163
$N = 6, 7$	3.8026	3.8568	2.4881	4.3163
$N = 5$	3.8026	3.8568	2.4889	4.3163
$N = 4$	3.8027	3.8569	2.4892	4.3163
$N = 3$	3.8027	3.8574	2.7023	4.3163
$N = 2$	3.8099	3.8656	2.7091	4.3174
TB	3.8076	3.8663	–	4.3203
EB	3.8455	3.9060	–	4.3271

[1] Flexural mode on plane *xz*.
[2] Flexural mode on plane *xy*.
[3] Torsional mode.
[4] Axial mode.

Table 4
Dimensionless natural frequencies, $E = E(y)$, $\nu = \nu(y)$, $\rho = \rho(y)$, $l/a = 5$, $n_1 = 1$.

$\overline{\omega}$	Mode I[1] $\times 10^{-1}$	Mode II[2] $\times 10^{-1}$	Mode III[3] $\times 10^{-1}$	Mode IV[4] $\times 10^{-1}$
FEM 3D[a]	1.4563	1.4726	4.9822	8.5820
FEM 3D[b]	1.4563	1.4726	4.9822	8.5821
FEM 3D[c]	1.4566	1.4727	4.9816	8.5826
$N \geqslant 10$	1.4562	1.4725	4.9824	8.5819
$N = 8, 9$	1.4562	1.4725	4.9825	8.5819
$N = 7$	1.4562	1.4725	4.9839	8.5819
$N = 6$	1.4562	1.4725	4.9840	8.5819
$N = 5$	1.4562	1.4726	4.9856	8.5819
$N = 4$	1.4563	1.4726	4.9873	8.5819
$N = 3$	1.4564	1.4735	5.4117	8.5822
$N = 2$	1.4648	1.4827	5.4251	8.5912
TB	1.4633	1.4861	–	8.6192
EB	1.5179	1.5436	–	8.6680

[1] Flexural mode on plane *xz*.
[2] Flexural mode on plane *xy*.
[3] Torsional mode.
[4] Axial mode.

order equal to eight in the case of slender beams and 10 for $l/a \leqslant 10$. Convergence is determined by the torsional mode, higher-order terms are required to accurately describe the in-plane cross-section warping. Torsional natural frequencies computed via a second- and a third-order theory differ from the FEM 3D[a] solution by about 9%. In the case of $N = 4$, the difference reduces to about 0.1%. Converged results differ from FEM 3D[a] solution by the last significant digit only. Classical models account for a rigid cross-section in its plane and, therefore, no torsional mode is present. EB yields very accurate flexural natural frequencies in the case of slender beams, whereas they differ by about 4.5% from the FEM reference solution in the case of $l/a = 5$.

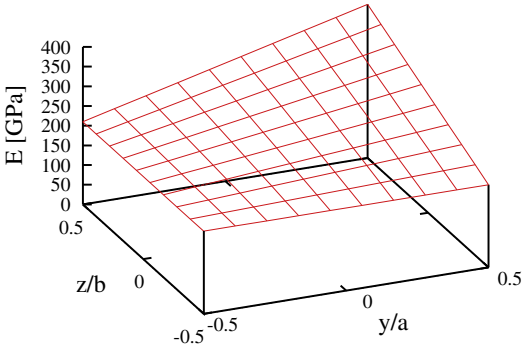

Fig. 2. Material power gradation law.

6.2. Material gradation along both cross-section directions

Changes in properties along both *y* and *z* directions are considered. Fig. 2 shows the variation of the Young's modulus. Due to the material gradation law, the cross-section is less stiff and heavier

Table 5
Dimensionless natural frequencies, $E = E(y,z)$, $\nu = \nu(y,z)$, $\rho = \rho(y,z)$, $l/a = 100$, $n_1 = n_2 = 1$.

$\overline{\omega}$	Mode I[1] $\times 10^2$	Mode II[2] $\times 10^2$	Mode III[3] $\times 1$	Mode IV[4] $\times 1$
FEM 3D[a]	3.2532	3.4149	2.1047	3.6968
FEM 3D[b]	3.2535	3.4155	2.1047	3.6968
FEM 3D[c]	3.2567	3.4165	2.1047	3.6968
$N \geqslant 8$	3.2520	3.4153	2.1048	3.6968
$N = 6, 7$	3.2520	3.4153	2.1054	3.6968
$N = 4, 5$	3.2520	3.4154	2.1061	3.6968
$N = 3$	3.2522	3.4155	2.2875	3.6968
$N = 2$	3.2526	3.4168	2.2906	3.6970
TB	3.2521	3.4153	–	3.6960
EB	3.2524	3.4157	–	3.6968

[1] Flexural mode on plane *xz*′.
[2] Flexural mode on plane *xy*′.
[3] Torsional mode.
[4] Axial mode.

Table 6
Dimensionless natural frequencies, $E = E(y,z)$, $\nu = \nu(y,z)$, $\rho = \rho(y,z)$, $l/a = 10$, $n_1 = n_2 = 1$.

$\bar{\omega}$	Mode I[1] $\times 1$	Mode II[2] $\times 1$	Mode III[3] $\times 10^{-1}$	Mode IV[4] $\times 10^{-1}$
FEM 3D[a]	3.2021	3.3596	2.1053	3.6916
FEM 3D[b]	3.2024	3.3595	2.1053	3.6916
FEM 3D[c]	3.2039	3.3586	2.1052	3.6916
$N \geqslant 8$	3.2019	3.3597	2.1053	3.6916
$N = 6, 7$	3.2019	3.3597	2.1059	3.6916
$N = 5$	3.2019	3.3597	2.1066	3.6916
$N = 4$	3.2019	3.3598	2.1068	3.6916
$N = 3$	3.2023	3.3599	2.2880	3.6916
$N = 2$	3.2077	3.3667	2.2911	3.6924
TB	3.2072	3.3654	–	3.6944
EB	3.2386	3.4018	–	3.6978

[1] Flexural mode on plane xz'.
[2] Flexural mode on plane xy'.
[3] Torsional mode.
[4] Axial mode.

Table 7
Dimensionless natural frequencies, $E = E(y,z)$, $\nu = \nu(y,z)$, $\rho = \rho(y,z)$, $l/a = 5$, $n_1 = n_2 = 1$.

$\bar{\omega}$	Mode I[1] $\times 10^{-1}$	Mode II[2] $\times 10^{-1}$	Mode III[3] $\times 10^{-1}$	Mode IV[4] $\times 10^{-1}$
FEM 3D[a]	1.2263	1.2837	4.2135	7.3520
FEM 3D[b]	1.2264	1.2837	4.2135	7.3520
FEM 3D[c]	1.2269	1.2833	4.2135	7.3523
$N \geqslant 10$	1.2262	1.2838	4.2136	7.3519
$N = 8, 9$	1.2262	1.2838	4.2137	7.3519
$N = 6, 7$	1.2262	1.2838	4.2149	7.3519
$N = 5$	1.2262	1.2838	4.2163	7.3519
$N = 4$	1.2263	1.2839	4.2178	7.3520
$N = 3$	1.2267	1.2840	4.5790	7.3522
$N = 2$	1.2338	1.2920	4.5850	7.3571
TB	1.2338	1.2917	–	7.3792
EB	1.2791	1.3442	–	7.4018

[1] Flexural mode on plane xz'.
[2] Flexural mode on plane xy'.
[3] Torsional mode.
[4] Axial mode.

than the case of variation along one direction only. Lower natural frequencies are, therefore, expected. Results are presented in Tables 5–7. Due to the material gradation law, cross-section axes of symmetry y' and z' are identified by a anti clock wise rotation of $\pi/4$ around the positive direction of x-axis. Modes I and II are two flexural modes on planes xz' and xy', respectively. Mode III is a torsional mode and Mode IV is an axial one. The same comments made in the case of Tables 2–4, are also valid in this case. Figs. 3 and 4 show the effect of the power law exponents n_1 and n_2 on the modal frequencies. Slender and deep beams are considered. The exponents are considered equal and as high as 10 and as low as 0.1. For all the considered modes, an increase in the power law exponent yields a decrease in the values of the frequencies. This is due to the fact that an increase in the value of the power law exponent results in a decrease in the elastic modulus and an increase in the density. The highest frequency values are obtained for a beam that is almost fully ceramic ($n_1 = n_2 = 0.1$), whereas the lowest frequency values are obtained for almost fully metallic beam ($n_1 = n_2 = 10$). All the UF model yield good results for flexural and axial modes. The torsional mode calls for a fourth-order theory, at lest. In the case of deep beams, natural flexural frequencies computed by EB differ from the reference three-dimensional solution by about 4%. Similar considerations hold in the case of material gradation along only a cross-section coordinate. Results are not reported for the sake of brevity.

7. Conclusions

A unified formulation of one-dimensional beam models has been proposed for the free vibration analysis of functionally graded beams. Via this approach, higher order models that account for non-classical effects such as shear deformations and in- and out-of-plane warping can be formulated straightforwardly. Euler–Bernoulli's and Timoshenko's classical models are regarded as

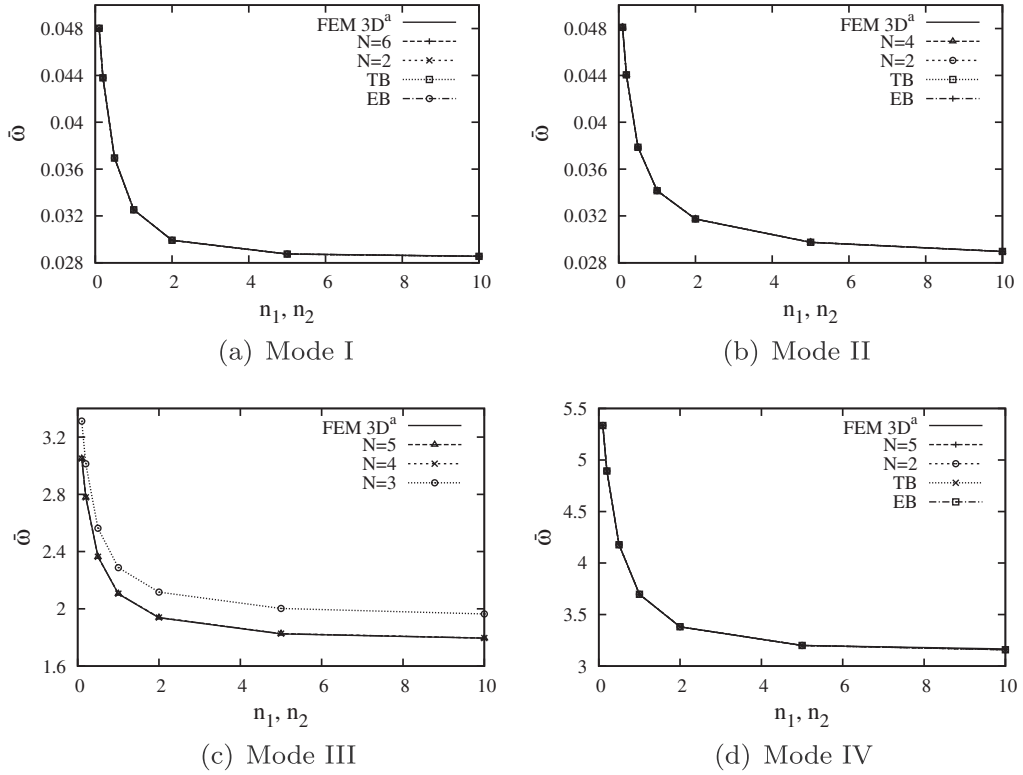

Fig. 3. Variation of the dimensionless natural frequencies versus the power law exponents n_1 and n_2, $l/a = 100$, $E = E(y,z)$, $\nu = \nu(y,z)$, $\rho = \rho(y,z)$.

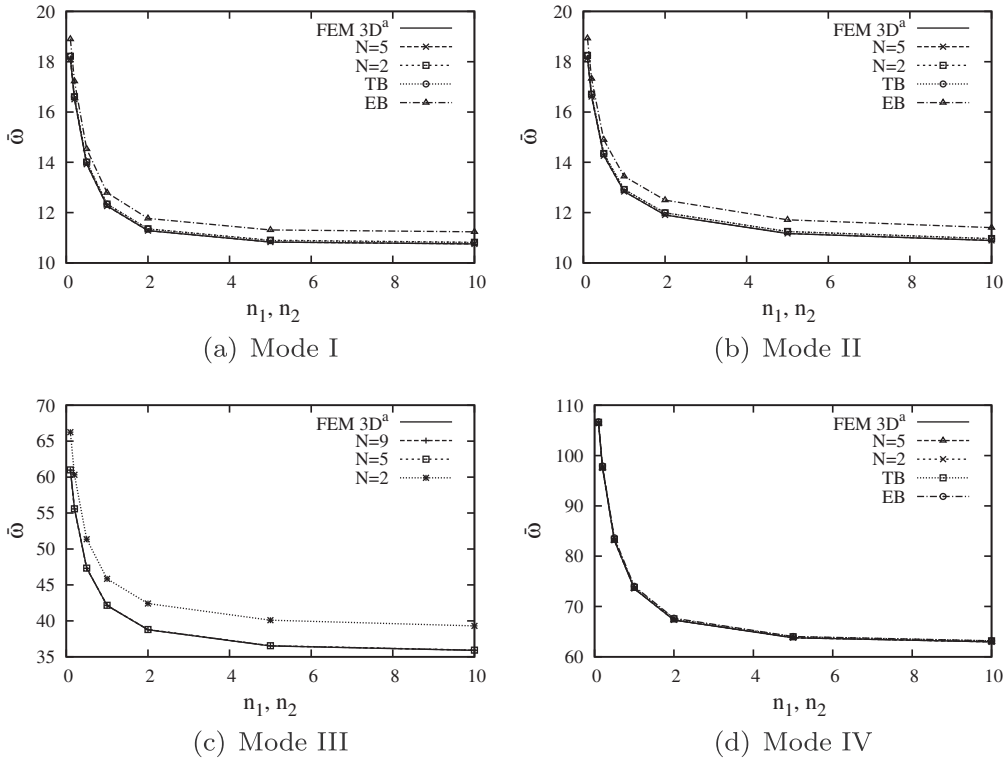

Fig. 4. Variation of the dimensionless natural frequencies versus the power law exponents n_1 and n_2, $l/a = 5$, $E = E(y,z)$, $\nu = \nu(y,z)$, $\rho = \rho(y,z)$.

particular cases. A closed form, Navier-type solution has been used. Young's modulus, Poisson's ratio and material density have been supposed to vary above the cross-section according to a power gradation law. Flexural, torsional and axial natural frequencies have been investigated. Results have been validated through comparison with three-dimensional FEM solutions obtained via the commercial code ANSYS. On the basis of the presented results, it can be concluded that the proposed formulation allows obtaining results as accurate as desired through an appropriate choice of the approximation order. The one-dimensional results match the three-dimensional FEM solutions. The efficiency of the proposed models is good since the computational time is less than a second for the highest considered approximation order, whereas for the three-dimensional FEM solution it can be three order of magnitude higher.

Acknowledgments

First author is supported by the Fonds National de la Recherche Luxembourg (FNR) via the CORE Project C09/MS/05 FUNCTIONALLY. Second author would like to thank FNR for his support via the AFR Grant PHD-MARP-03.

References

[1] Şimşek M. Fundamental frequency analysis of functionally graded beams by using different higher-order beam theories. Nuclear Engineering and Design 2010;240:697–705.
[2] Kapuria S, Bhattacharyya M, Kumarb AN. Bending and free vibration response of layered functionally graded beams: A theoretical model and its experimental validation. Composite Structures 2008;82(3):390–402.
[3] Xiang HJ, Yang J. Free and forced vibration of a laminated fgm timoshenko beam of variable thickness under heat conduction. Composites:Part B 2008;39:292–303.
[4] Aydogdu M, Taskin V. Free vibration analysis of functionally graded beams with simply supported edges. Materials and Design 2007;28:1651–6.
[5] Li XF. A unified approach for analyzing static and dynamic behaviors of functionally graded timoshenko and euler-bernoulli beams. Journal of Sound and Vibration 2008;318(4–5):1210–29.
[6] Sina SA, Navazi HM, Haddadpour H. An analytical method for free vibration analysis of functionally graded beams. Materials and Design 2009;30:741–7.
[7] Alshorbagy AE, Eltaher MA, Mahmoud FF. Free vibration characteristics of a functionally graded beam by finite element method. Applied Mathematical Modelling 2011;35:412–25.
[8] Murin J, Aminbaghai M, Kutis V. Exact solution of the bending vibration problem of fgm beams with variation of material properties. Engineering Structures 2010;32:1631–40.
[9] Carrera E. Theories and finite elements for multilayered plates and shells: a unified compact formulation with numerical assessment and benchmarking. Archives of Computational Methods in Engineering 2003;10(3):215–96.
[10] Carrera E, Giunta G. Hierarchical evaluation of failure parameters in composite plates. AIAA Journal 2009;47(3):692–702.
[11] Carrera E, Giunta G. Exact, hierarchical solutions for localised loadings in isotropic, laminated and sandwich shells. Journal of Pressure Vessel Technology 2009;131(4):0412021–04120214.
[12] Giunta G, Belouettar S, Carrera E. Analysis of fgm beams by means of classical and advanced theories. Mechanics of Advanced Materials and Structures 2010;17(8):622–35.
[13] Carrera E, Giunta G. Refined beam theories based on a unified formulation. International Journal of Applied Mechanics 2010;2(1):117–43.
[14] Carrera E, Giunta G, Nali P, Petrolo M. Refined beam elements with arbitrary cross-section geometries. Computers and Structures 2010;88(5-6):283–93.
[15] G. Giunta, F. Biscani, E. Carrera, and S. Belouettar, Analysis of thin-walled beams via a one-dimensional unified formulation, International Journal of Applied Mechanics, at press time.
[16] Praveen GN, Reddy JN. Nonlinear transient thermoelastic analysis of functionally graded ceramic-metal plates. International Journal of Solids and Structures 1998;35(33):4457–76.
[17] Chakraborty A, Gopalakrishnan S, Reddy JN. A new beam finite element for the analysis of functionally graded materials. International Journal of Mechanical Sciences 2003;45(3):519–39.
[18] Cowper GR. The shear co-efficient in timoshenko beam theory. Journal of Applied Mechanics 1966;33(10):335–40.
[19] Murty AVK. Analysis of short beams. AIAA Journal 1970;8(11):2098–100.
[20] Carrera E, Brischetto S. Analysis of thickness locking in classical, refined and mixed multilayered plate theories. Composite Structures 2008;82(4):549–62.
[21] Carrera E, Brischetto S. Analysis of thickness locking in classical, refined and mixed theories for layered shells. Composite Structures 2008;85(1):83–90.
[22] ANSYS v10.0 theory manual. ANSYS Inc., Southpointe, PA, 2006.
[23] Madenci E, Guven I. The Finite Element Method and Applications in Engineering using ANSYS®. New York, USA: Springer; 2006.
[24] Barbero EJ. Finite element analysis of composite materials. New York: CRC Press; 2008.